CrossMark

TECHNICAL ARTICLE

Structure analysis of $CaTi_{1-x}Sn_xO_3$ ($x = 0.0–1.0$) solid solutions

Naoki Takani, and Hisanori Yamane[a)]
Institute of Multidisciplinary Research for Advanced Materials, Tohoku University, 2-1-1 Katahira, Aoba-ku, Sendai 980-8577, Japan

(Received 24 October 2013; accepted 19 December 2013)

$CaTi_{1-x}Sn_xO_3$ ($x = 0.0–1.0$) solid solutions were prepared by solid-state reaction at 1450 °C. Rietveld refinement of their powder X-ray diffraction patterns revealed that all the solid solutions crystallized in orthorhombic cells with the perovskite-type structure, the space group *Pbnm*. The refined unit-cell parameters linearly increased with nominal tin contents *x*. © *2014 International Centre for Diffraction Data*. [doi:10.1017/S0885715614000074]

Key words: calcium titanate stannate, perovskite-type structure, solid solutions, powder diffraction, Rietveld analysis

I. INTRODUCTION

Recently, polycrystalline garnet-type solid solutions of $Ca_3Sn_{2-x}Ti_xAl_2O_{12}$ ($x = 0.5 - 1.5$) have been synthesized in the $CaO–Al_2O_3–TiO_2–SnO_2$ system by solid-state reaction, and the crystal structures and photoluminescence properties of the solid solutions have been investigated (Yamane and Kawano, 2011). In the process of this research, a secondary phase that seemed to be a $CaTiO_3–CaSnO_3$ solid solution was found by powder X-ray diffraction (XRD). Isaeva *et al.* (1972) reported changes in the *a*-axis cell parameter of $CaTi_{1-x}Sn_xO_3$ solid solutions and their dielectric losses at 10 GHz and 300 K. However, the solid solutions crystallize in orthorhombic cells and there have been no detailed structural studies of $CaTi_{1-x}Sn_xO_3$ including the information on the *b*- and *c*-axes. The crystal structures of both $CaTiO_3$ and $CaSnO_3$ are of the same orthorhombic perovskite type (space group *Pbnm*) and composed of TiO_6 and SnO_6 octahedra, respectively, by sharing their corners (Vegas *et al.*, 1986). TiO_2 and SnO_2, consisting of TiO_6 and SnO_6 octahedra, respectively, have the same rutile-type crystal structure (tetragonal, space group $P4_2/mnm$), and spinodal decomposition is known to occur in $Ti_{1-x}Sn_xO_2$ solid solutions (Park *et al.*, 1975). In this study, $CaTi_{1-x}Sn_xO_3$ solid solutions were prepared and their crystal structures were investigated by Rietveld refinement using powder XRD patterns.

II. EXPERIMENTAL

A. Synthesis

Starting materials were powders of $CaCO_3$ (99.99%, Rare Metallic), TiO_2 (99.99%, Rare Metallic), and SnO_2 (99.998%, Kojundo Chemical Laboratory Co.). The $CaCO_3$ powder was dried at 150 °C before mixing. The powders were weighed to the molar ratios of Ca, Ti, and Sn corresponding to the formula $CaTi_{1-x}Sn_xO_3$ ($x = 0.0–1.0$), mixed in an agate mortar with a pestle, and pressed into pellets. The pellets were placed on a platinum–rhodium plate and calcined at 1200 °C for 12 h in air using an electric furnace. The calcined pellets were ground, mixed, pelletized, and then heated at 1450 °C for 12 h.

B. Data collection

The obtained polycrystalline pellets were powdered and powder XRD pattern measurements were conducted at a step width of 0.02° at 2θ using CuK_α radiation with a graphite monochromator mounted on a powder diffractometer (Rigaku, Model RINT2200). The crystal structure parameters of the solid solutions were refined using the RIETAN-FP program (Izumi and Momma, 2007). Illustrations of the crystal structures and calculations of the interatomic distances, bond angles, and coordination polyhedron volumes were performed using the Visualization for Electronic and Structural Analysis (VESTA) program (Momma and Izumi, 2008).

III. RESULTS AND DISCUSSION

Single phases of $CaTiO_3$ ($x = 0.0$) and $CaSnO_3$ ($x = 1.0$) were synthesized by heating powders at 1450 °C for 12 h. Powder XRD reflections of the samples prepared with $x =$ 0.1–0.9 under the same heating condition were indexed with orthorhombic cell parameters (space group, *Pbnm*). The crystal structure of $CaTiO_3$ reported by Mitchell and Liferovich (2004) was used as a starting model for Rietveld refinement. Since all the obtained samples were single phases, the occupancies of Ti and Sn atoms in the Ti/Sn site were fixed corresponding to the starting compositions of $x = Sn/(Ti + Sn)$. Table I lists crystallographic characteristics of $CaTi_{1-x}Sn_xO_3$. The final *R* and *S* indices of the refinement were $R_{wp} =$ 10.931–13.916, $R_p = 7.686–9.676\%$, $R_I = 1.548–4.104\%$, $R_F = 1.277–2.828\%$, and $S = 1.164 - 1.475$. Figure 1 shows the observed and calculated powder XRD patterns of $CaTi_{0.8}Sn_{0.2}O_3$ as an example. The largest misfit was observed around the diffraction peak of 121 with the highest intensity at $2\theta = 32.88°$. The full-width at half-maximum (FWHM) fitted by Rietveld analysis in the 2θ range of 20–140° was from 0.11° to 0.75° which was larger than the FWHM of $CaTiO_3$ from 0.09° to 0.32°. Such diffraction peak broadening suggested the microstrain in the solid solution. The crystal

[a)]Author to whom correspondence should be addressed. Electronic mail: yamane@tagen.tohoku.ac.jp

https://doi.org/10.1017/S0885715614000074 Published online by Cambridge University Press

https://doi.org/10.1017/S0885715614000074 Published online by Cambridge University Press

TABLE I. Crystallographic characteristics of $CaTi_{1-x}Sn_xO_3$.

Formula		$CaTiO_3$	$CaTi_{0.9}Sn_{0.1}O_3$	$CaTi_{0.8}Sn_{0.2}O_3$	$CaTi_{0.7}Sn_{0.3}O_3$	$CaTi_{0.6}Sn_{0.4}O_3$	$CaTi_{0.5}Sn_{0.5}O_3$	$CaTi_{0.4}Sn_{0.6}O_3$	$CaTi_{0.3}Sn_{0.7}O_3$	$CaTi_{0.2}Sn_{0.8}O_3$	$CaTi_{0.1}Sn_{0.9}O_3$	$CaSnO_3$
Cell	a	5.380 79(12)	5.396 51(19)	5.410 01(2)	5.4237(2)	5.4370(2)	5.448 97(16)	5.4643(2)	5.479 58(19)	5.491 12(14)	5.502 12(10)	5.515 05(6)
parameter	b	5.442 73(12)	5.464 95(19)	5.4878(2)	5.5098(2)	5.5333(2)	5.554 85(16)	5.5792(2)	5.602 22(19)	5.622 99(15)	5.642 61(11)	5.664 37(6)
(Å)	c	7.641 38(16)	7.6689(3)	7.6924(3)	7.7166(3)	7.7411(3)	7.7636(2)	7.7902(3)	7.8160(3)	7.8381(2)	7.859 28(15)	7.882 51(9)
Cell volume ($Å^3$)		223.787(8)	226.170(14)	228.382(16)	230.600(17)	232.890(17)	234.989(12)	237.492(16)	239.934(14)	242.012(11)	244.002(8)	246.244(5)
R indices	R_{wp}	13.916	12.634	12.008	11.679	11.487	11.675	10.931	11.551	11.957	12.682	13.539
	R_p	9.532	9.193	8.479	8.363	8.297	8.439	7.686	8.076	8.382	8.844	9.676
	R_I	3.031	3.225	2.348	1.621	1.874	2.493	1.745	1.548	1.676	3.076	4.104
	R_F	2.828	2.408	2.231	1.633	1.761	2.098	1.411	1.277	1.370	2.135	2.831
Good-of-fit	S	1.189	1.168	1.164	1.178	1.185	1.212	1.185	1.235	1.291	1.359	1.475
Atom												
Ca	g	1	1	1	1	1	1	1	1	1	1	1
	x	−0.0070(4)	−0.0080(5)	−0.0085(5)	−0.0102(5)	−0.0088(6)	−0.0113(6)	−0.0101(6)	−0.0121(6)	−0.0132(6)	−0.0133(6)	−0.0144(6)
	y	0.035 41(19)	0.0369(2)	0.0390(2)	0.0414(2)	0.0431(2)	0.0450(2)	0.0460(2)	0.0475(3)	0.0490(3)	0.0492(3)	0.0528(3)
	z	1/4	1/4	1/4	1/4	1/4	1/4	1/4	1/4	1/4	1/4	1/4
	B ($Å^2$)	0.58(2)	0.68(3)	0.69(3)	0.63(3)	0.65(3)	0.62(3)	0.68(3)	0.61(4)	0.42(4)	0.26(4)	0.39(4)
Sn/Ti	g	1.0/0.0	0.9/0.1	0.8/0.2	0.7/0.3	0.6/0.4	0.5/0.5	0.4/0.6	0.3/0.7	0.2/0.8	0.1/0.9	0.0/1.0
	x	0	0	0	0	0	0	0	0	0	0	0
	y	1/2	1/2	1/2	1/2	1/2	1/2	1/2	1/2	1/2	1/2	1/2
	z	0	0	0	0	0	0	0	0	0	0	0
	B ($Å^2$)	0.408(19)	0.408(19)	0.332(19)	0.288(18)	0.263(18)	0.236(17)	0.283(16)	0.268(16)	0.15(15)	0.109(14)	0.099(12)
O1	g	1	1	1	1	1	1	1	1	1	1	1
	x	0.0754(9)	0.0746(9)	0.0829(10)	0.0836(11)	0.0862(11)	0.0884(11)	0.0895(11)	0.0980(12)	0.0970(12)	0.1000(12)	0.1032(12)
	y	0.4845(7)	0.4834(7)	0.4791(8)	0.4775(9)	0.4755(10)	0.4724(10)	0.4725(10)	0.4667(11)	0.4643(11)	0.4663(12)	0.4647(12)
	z	1/4	1/4	1/4	1/4	1/4	1/4	1/4	1/4	1/4	1/4	1/4
	B ($Å^2$)	0.51(10)	0.54(12)	0.66(13)	0.836(11)	0.66(14)	0.66	0.59(13)	0.74(15)	0.80(16)	0.80	0.80
O2	g	1	1	1	1	1	1	1	1	1	1	1
	x	0.7122(5)	0.7111(6)	0.7086(6)	0.7077(7)	0.7078(7)	0.7052(7)	0.7054(7)	0.7043(7)	0.7009(8)	0.7031(8)	0.6990(8)
	y	0.2889(5)	0.2901(6)	0.2913(6)	0.2913(6)	0.2927(7)	0.2913(7)	0.2938(6)	0.2938(7)	0.2937(7)	0.2954(8)	0.2953(8)
	z	0.0359(4)	0.0373(5)	0.0386(5)	0.0410(5)	0.0434(6)	0.0447(6)	0.0459(5)	0.0473(6)	0.0485(6)	0.0496(6)	0.0494(6)
	B ($Å^2$)	0.29(7)	0.49(8)	0.30(8)	0.13(9)	0.42(10)	0.42[a]	0.07(9)	0.10(9)	0.27(10)	0.27[b]	0.27[b]

[a]Constrained the value of O1 and O2 with those of $CaTi_{0.6}Sn_{0.4}O_3$.
[b]Constrained the value of O1 and O2 with those of $CaTi_{0.2}Sn_{0.8}O_3$.

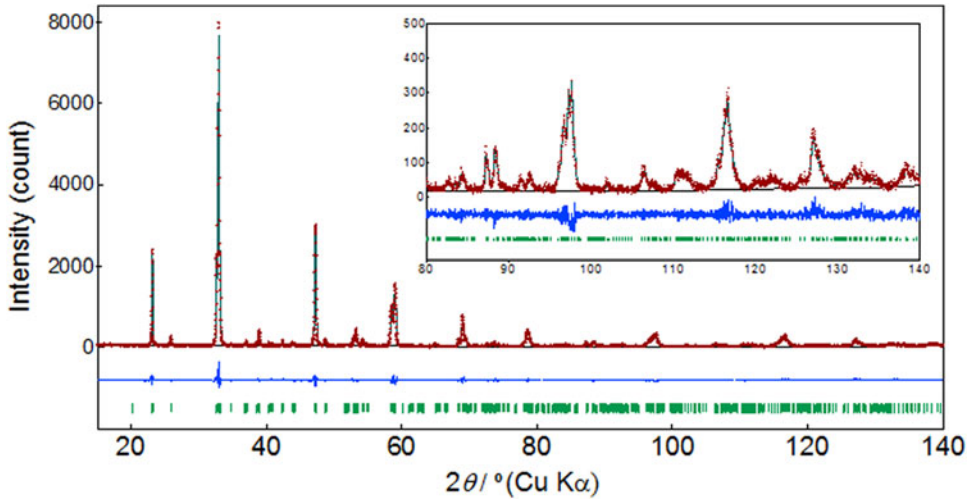


Figure 1. (Color online) Rietveld refinement plot of the powder diffraction data for $CaTi_{0.8}Sn_{0.2}O_3$. The bars indicate the allowed Bragg reflections for the *Pbnm* structure.

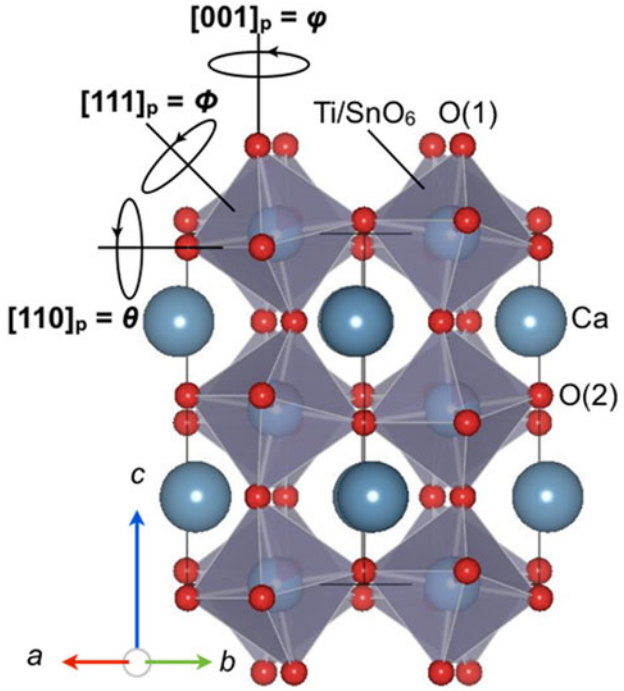


Figure 2. (Color online) The crystal structure of $CaTi_{0.8}Sn_{0.2}O_3$ in a representation using Ti/Sn-centered oxygen polyhedra.

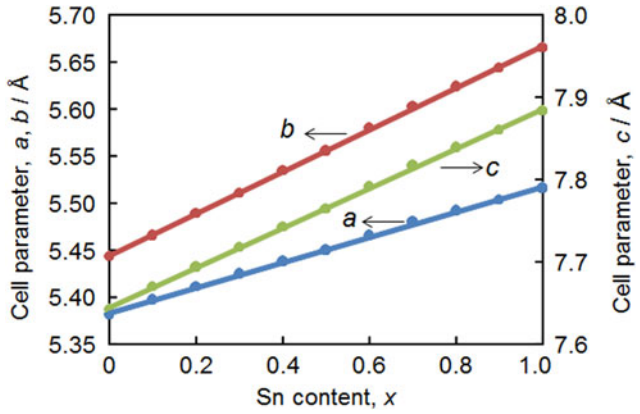


Figure 3. (Color online) Unit-cell parameters of the $CaTi_{1-x}Sn_xO_3$ solid solutions.

structure of $CaTi_{0.8}Sn_{0.2}O_3$ is illustrated in Figure 2 with Ti/Sn-centered oxygen polyhedra (Ti/SnO_6).

The cell parameters of $CaTiO_3$ were refined to be a = 5.380 79(12), b = 5.442 73(12), and c = 7.641 38(16) Å and were in good agreement with reported values (a = 5.381 59 (6), b = 5.442 81(7), and c = 7.642 07(10) Å) (Mitchell and Liferovich, 2004). Refined $CaSnO_3$ cell parameters were a = 5.515 05(6), b = 5.664 37(6), and c = 7.882 51(9) Å, comparable to those (a = 5.5142(2), b = 5.6634(2), and c = 7.881 62(17) Å) reported by Zhao *et al.* (2004). Figure 3 shows the cell parameters refined by Rietveld analysis. As x increased, the cell parameters of the a-, b-, and c-axes linearly increased. Figure 4 plots the cell parameters normalized with the parameters of $CaTiO_3$ (x = 0.0) as a function of the Sn content x. The rate of the b-axis increase ($b_{x=1.0}/b_{x=0.0}$ = 1.4) was the largest. The interatomic distances and bond angles of $CaTi_{1-x}Sn_xO_3$ are shown in Table II. CaO_8 and CaO_{12} polyhedral volumes (V_{CaO8}, V_{CaO12}), Ti/SnO_6 octahedral volume ($V_{Ti/SnO6}$), the averages of Ca–O distances in the first and second coordination spheres (L_{CaO8}, L_{CaO12}) and in between the spheres ($L_{CaO8–CaO12}$), and the average of Ti/Sn–O bonds ($L_{Ti/SnO6}$) are listed in Table III. The bond valence sums (BVSs) of the Ti/SnO_6 octahedron and CaO_{12} polyhedra are listed in Table IV. The values of V_{CaO8}, V_{CaO12}, $V_{Ti/SnO6}$, L_{CaO8}, $L_{CaO12–CaO8}$, L_{CaO12}, and $L_{Ti/SnO6}$ are plotted as functions of x in Figure 5.

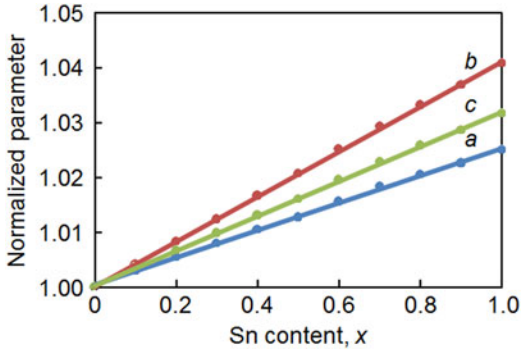


Figure 4. (Color online) Normalized unit-cell parameters of the $CaTi_{1-x}Sn_xO_3$ solid solutions.

https://doi.org/10.1017/S0885715614000074 Published online by Cambridge University Press

TABLE II. Selected bond lengths (Å) and angles (°) of $CaTi_{1-x}Sn_xO_3$.

	$x = 0.0$	$x = 0.1$	$x = 0.2$	$x = 0.3$	$x = 0.4$	$x = 0.5$	$x = 0.6$	$x = 0.7$	$x = 0.8$	$x = 0.9$	$x = 1.0$
Ca–O1	2.339(5)	2.357(6)	2.326(6)	2.341(7)	2.328(7)	2.340(7)	2.335(7)	2.314(7)	2.334(7)	2.322(7)	2.322(7)
Ca–O1	2.484(4)	2.480(4)	2.465(5)	2.456(5)	2.447(5)	2.435(6)	2.441(6)	2.425(6)	2.413(6)	2.435(7)	2.422(7)
2 × Ca–O2	2.387(3)	2.383(4)	2.380(4)	2.377(4)	2.377(4)	2.376(5)	2.377(4)	2.375(4)	2.370(5)	2.371(5)	2.380(5)
2 × Ca–O2	2.620(3)	2.622(4)	2.628(4)	2.615(4)	2.615(5)	2.607(5)	2.619(4)	2.613(5)	2.618(5)	2.616(5)	2.624(5)
2 × Ca–O2	2.660(3)	2.673(4)	2.678(4)	2.700(4)	2.715(5)	2.730(5)	2.738(4)	2.756(5)	2.764(5)	2.781(5)	2.774(5)
Ca–O1	3.071(5)	3.072(6)	3.125(6)	3.130(7)	3.162(7)	3.170(7)	3.193(7)	3.242(7)	3.241(7)	3.262(7)	3.285(7)
Ca–O1	3.031(4)	3.058(4)	3.112(5)	3.148(5)	3.183(5)	3.227(6)	3.246(6)	3.309(6)	3.343(6)	3.347(7)	3.393(7)
2 × Ca–$O2_{max}$	3.226(3)	3.258(4)	3.293(4)	3.330(4)	3.360(4)	3.392(5)	3.417(4)	3.450(5)	3.483(5)	3.498(5)	3.533(5)
2 × Ca–Ti/Sn_{min}	3.1694(8)	3.1755(9)	3.1780(10)	3.1797(11)	3.1841(11)	3.1872(11)	3.1955(11)	3.2014(11)	3.2058(11)	3.2152(12)	3.2106(12)
2 × Ti/Sn–O1	1.9548(10)	1.9611(10)	1.9780(13)	1.9855(14)	1.9958(15)	2.006(2)	2.0138(15)	2.035(2)	2.041(2)	2.049(2)	2.061(2)
2 × Ti/Sn–O2	1.948(3)	1.957(3)	1.971(3)	1.984(4)	1.988(4)	1.997(4)	2.011(4)	2.024(4)	2.022(4)	2.038(4)	2.038(4)
2 × Ti/Sn–O2	1.963(3)	1.973(3)	1.979(3)	1.986(3)	2.003(4)	2.011(4)	2.019(4)	2.024(4)	2.046(4)	2.044(4)	2.062(4)
O1–Ti/Sn–O1	180	180	180	180	180	180	180	180	180	180	180
2 × O1–Ti/Sn–O2	88.92(13)	89.19(13)	88.26(14)	88.55(14)	88.59(15)	88.38(15)	88.52(14)	87.42(15)	87.6(2)	87.7(2)	87.4(2)
2 × O1–Ti/Sn–O2	90.12(13)	89.62(14)	90.07(14)	89.51(15)	89.1(2)	88.9(2)	88.79(15)	89.1(2)	88.6(2)	88.8(2)	89.3(2)
2 × O1–Ti/Sn–O2	91.08(13)	90.81(13)	91.74(14)	91.45(14)	91.41(15)	91.62(15)	91.48(14)	92.58(15)	92.4(2)	92.3(2)	92.6(2)
2 × O1–Ti/Sn–O2	89.88(13)	90.38(14)	89.93(14)	90.49(15)	90.9(2)	91.1(2)	91.21(15)	90.9(2)	91.4(2)	91.2(2)	90.7(2)
2 × O2–Ti/Sn–O2	89.45(11)	89.42(12)	89.47(12)	89.42(13)	89.28(13)	89.42(13)	89.31(13)	89.31(13)	89.43(14)	89.27(14)	89.54(14)
2 × O2–Ti/Sn–O2	90.55(11)	90.58(12)	90.53(12)	90.58(13)	90.72(13)	90.57(13)	90.69(13)	90.69(13)	90.57(14)	90.73(14)	90.46(14)
Ti/Sn–O1–Ti/Sn	155.5(2)	155.7(2)	152.9(2)	152.6(2)	151.7(2)	150.8(2)	150.5(2)	147.6(2)	147.6(2)	147.0(2)	146.0(2)
Ti/Sn–O2–Ti/Sn	156.3(2)	155.5(2)	154.5(2)	153.7(2)	152.7(2)	152.2(2)	151.4(2)	150.9(2)	150.0(2)	149.7(2)	149.2(2)

The increase of Ti/Sn–O bond lengths by substitution of Ti^{4+} for Sn^{4+} corresponds to the difference of ionic radii for Ti^{4+} and Sn^{4+} (six-coordinate: Ti^{4+} 0.605 Å, Sn^{4+} 0.69 Å (Shannon, 1976)). $L_{Ti/SnO6}$ linearly changed from the average of Ti–O distances in $CaTiO_3$ ($L_{TiO6(x=0.0)}$ = 1.955 Å) to that of Sn–O distances in $CaSnO_3$ ($L_{SnO6(x=1.0)}$ = 2.054 Å). The increase rate of L_{SnO6}/L_{TiO6} was 1.05. In accordance with this change, the volume of Ti/SnO_6 octahedra increased from 9.96 to 11.53 $Å^3$. The BVS calculated for the Ti/Sn site with the Ti^{4+} bond valence parameter (Brese and O'Keeffe, 1991) monotonously decreased from 4.11 to 3.15 with increasing x from 0 to 1.0. The BVS with Sn^{4+} at x = 1.0 was 4.01, which was almost in agreement with the valence of Sn.

V_{CaO8} and L_{CaO8} did not change so much by substitution of Sn^{4+} for Ti^{4+}. L_{CaO8} lengths are in the range of $L_{CaO8(x=0.0)}$ = 2.520 Å to $L_{CaO8(x=1.0)}$ = 2.538 Å ($L_{CaO8(x=1.0)}/L_{CaO8(x=0.0)}$ = 1.01). V_{CaO8} changed from 25.21 to 26.77 $Å^3$. L_{CaO12} increased from 2.726 to 2.837 Å with the $L_{CaO12(x=1.0)}/L_{CaO12(x=0.0)}$ rate of 1.04, close to the L_{SnO6}/L_{TiO6} rate of 1.05. As seen in each interatomic distance, the increasing rates of the distances with x become larger in the following order: $L_{CaO8–CaO12}$, $L_{Ti/SnO6}$, and L_{CaO8}. The BVSs of Ca calculated for the CaO_{12} polyhedra were consistent with the valence of Ca.

The tilt angles of the Ti/SnO_6 octahedra about the pseudocubic $[110]_p$, $[001]_p$, and $[111]_p$ axes (Table III and Figure 2) were calculated from the bond angles by following Zhao *et al.* (1993). As shown in Figure 6, the Ti/SnO_6 tilt angles $[110]_p$, $[001]_p$, and $[111]_p$ increase uniformly with x from 12.3° to 17.0°, from 8.1° to 9.6°, and from 14.7° to 19.9°, respectively.

Judging from the results mentioned above, the lattice parameters and atomic arrangements of $CaTi_{1-x}Sn_xO_3$ solid solutions gradually and continuously changed from the structure of $CaTiO_3$ to $CaSnO_3$. Phase separation similar to that observed in $Ti_{1-x}Sn_xO_2$ solid solutions was not found in $CaTi_{1-x}Sn_xO_3$ solid solutions.

$CaTi_{1-x}Sn_xO_3$ solid solutions were sintered for measurement of capacitance (C) and dielectric loss (D) at 100 Hz–1 MHz and room temperature using an LCR (inductance (L), capacitance (C), resistance (R)) meter. The sintering conditions of the sample with x = 0.0–0.2, 0.4–0.6, and 0.8 were at 1550 °C for 24 h, at 1600 °C for 2 h, and at 1700 °C for 2 h, respectively. The ceramic bulk sample of $CaSnO_3$ (x = 1.0) was prepared by covering the sample pellet with SnO_2 powder and by heating at 1700 °C for 2 h. The relative densities were more than 82% for the ceramics with x = 0.0 – 0.8 and 72% for x = 1.0. The dielectric constants of $CaTiO_3$ were 172–169 at 100 Hz–1 MHz and in good agreement with the reported value (170 at 5 GHz) (Jancar *et al.*, 2003). The dielectric constants and dielectric losses of $CaSnO_3$ reported by Coffeen *et al.* (1953) were 17 and 0.0004 at 1 kHz and 14 and 0.000 at 10 kHz, whereas those reported by Mandal *et al.* (1995) were 130 and 0.8 at 10 kHz, and 70 and 0.3 at 100 kHz. Both of these reports did not include information about the densities of the samples. The dielectric constants of $CaSnO_3$ measured at room temperature at 100 Hz–1 MHz in our study were 37–13, values close to the former ones. The dielectric constants of $CaTi_{1-x}Sn_xO_3$ ceramics decreased with x. The changes of $CaTi_{1-x}Sn_xO_3$ dielectric loss with x had a tendency similar to that reported by Isaeva *et al.* (1972).

https://doi.org/10.1017/S0885715614000074 Published online by Cambridge University Press

TABLE III. Crystal chemistry of $CaTi_{1-x}Sn_xO_3$.

x	V_{CaO8} (Å^3)	L_{CaO8} (Å)	V_{CaO12} (Å^3)	$L_{CaO8-CaO12}$ (Å)	L_{CaO12} (Å)	$V_{Ti/SnO6}$ (Å^3)	$L_{Ti/SnO6}$ (Å)	$[110]_p$	$[001]_p$	$[111]_p$
0.0	25.21	2.520	47.43	3.139	2.726	9.96	1.955	12.3	8.10	14.7
0.1	25.44	2.524	47.95	3.162	2.737	10.09	1.964	12.2	8.75	14.9
0.2	25.48	2.521	48.42	3.206	2.749	10.28	1.976	13.6	8.43	15.9
0.3	25.67	2.523	48.86	3.235	2.760	10.43	1.985	13.7	8.91	16.3
0.4	25.79	2.524	49.31	3.266	2.771	10.59	1.996	14.2	9.31	16.9
0.5	25.98	2.525	49.74	3.295	2.782	10.73	2.005	14.6	9.33	17.3
0.6	26.16	2.530	50.27	3.318	2.793	10.89	2.014	14.8	9.81	17.7
0.7	26.23	2.528	50.74	3.363	2.806	11.10	2.028	16.2	8.98	18.5
0.8	26.43	2.531	51.20	3.388	2.817	11.24	2.036	16.2	9.70	18.8
0.9	26.57	2.537	51.57	3.401	2.825	11.37	2.044	16.5	9.68	19.1
1.0	26.77	2.538	52.08	3.436	2.837	11.53	2.054	17.0	9.64	19.5

Notes: V_{CaO8} and V_{CaO12} are volumes (Å^3) of polyhedra with Ca in 8- and 12-fold coordination, respectively. $V_{Ti/SnO6}$ is the volume (Å^3) of the Ti/SnO_6 octahedron. $L_{Ti/SnO6}$ is the mean bond length (Å) for the Ti/SnO_6 octahedron, L_{CaO8}, L_{CaO12}, and $L_{CaO8-CaO12}$ are the mean Ca–O distances in the first (CaO_8) and second (CaO_{12}) spheres and in between the spheres (CaO_8-CaO_{12}). $[110]_p$, $[001]_p$, and $[111]_p$ are octahedral tilt angles (°); all tilt angles are determined from bond angles.

TABLE IV. BVSs of the Ti/SnO_6 octahedron and CaO_{12} polyhedron.

x	BVS_{TiO6}	BVS_{CaO12}
0.0	4.11	2.08
0.1	4.02	2.05
0.2	3.88	2.06
0.3	3.79	2.05
0.4	3.68	2.05
0.5	3.59	2.03
0.6	3.50	2.01
0.7	3.37	2.03
0.8	3.29	2.01
0.9	3.22	2.01
1.0	3.15	1.98

BVS, $\Sigma_j \exp[(l_0-l_{ij})/B]$; l_0, bond length (Å), $B = 0.37$ Å; l_0, bond valence parameter (Ti^{4+}, 1.815 Å; Ca^{2+}, 1.967 Å) (Brese and O'Keeffe, 1991).

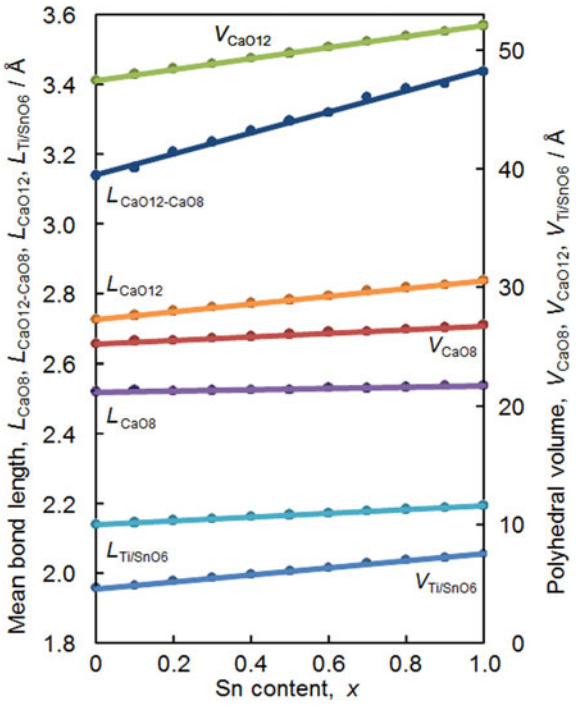


Figure 5. (Color online) Mean bond lengths and polyhedral volumes of CaO_8 and CaO_{12} polyhedral volumes (V_{CaO8}, V_{CaO12}), Ti/SnO_6 octahedral volume ($V_{Ti/SnO6}$), the averages of Ca–O distances in the first and second coordination spheres (L_{CaO8}, L_{CaO12}) and in between the spheres ($L_{CaO8-CaO12}$), and the average of Ti/Sn–O bonds ($L_{Ti/SnO6}$) in the $CaTi_{1-x}Sn_xO_3$ solid solutions.

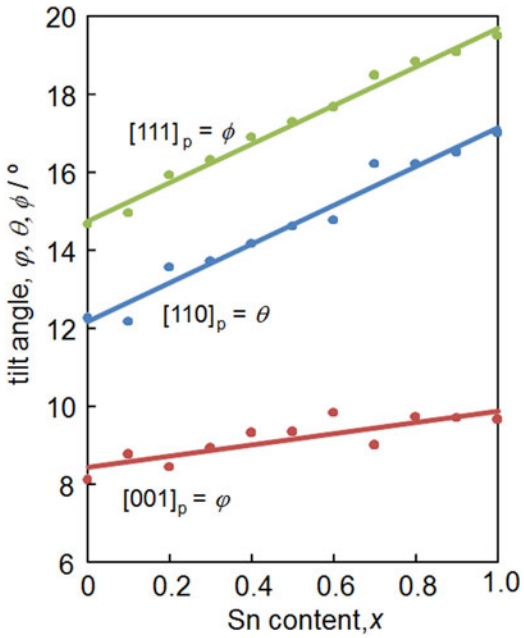


Figure 6. (Color online) Octahedral tilt angles (°) $[110]_p$, $[001]_p$, and $[111]_p$ in the $CaTi_{1-x}Sn_xO_3$ solid solutions.

IV. CONCLUSION

The crystal structures of $CaTi_{1-x}Sn_xO_3$ ($x = 0.0$–1.0) solid solutions prepared by solid-state reaction at 1450 °C for 12 h were investigated by the Rietveld analysis of powder XRD patterns. The parameters of the orthorhombic cells (space group *Pbnm*) and the Ti/Sn–O bond lengths were linearly increased by substitution of Sn for Ti.

Brese, N. E and O'Keeffe, M. (**1991**). "Bond-valence parameters for solids," Acta Crystallogr. B **47**, 192–197.

Coffeen, W. W. (**1953**). "Ceramic and dielectric properties of the stannates," J. Am. Ceram. Soc. **36**, 207–214.

Isaeva, V. F., Lifshits, Y. A., Fridberg, I. D., and Cherkudinov, A. S. (**1972**). "Systems of oxides used in electrical ceramics and their properties at high frequencies," Vysokotemp. Khim. Silikat. Okislov, Tr. Vses. Soveshch. **3**, 112–116.

Izumi, F. and Momma, K. (**2007**). "Three-dimensional visualization in power diffraction," Solid State Phenom. **130**, 15–20.

Jancar, B., Suvorov, D., Valant, M., and Drazic, G. (**2003**). "Characterization of $CaTiO_3$–$NdAlO_3$ dielectric ceramics," J. Eur. Ceram. Soc. **23**, 1391–1400.

https://doi.org/10.1017/S0885715614000074 Published online by Cambridge University Press

Mandal, K. D., Sastry, M. S., and Parkash, O. (**1995**). "Preparation and characterization of calcium stannate," J. Mater. Sci. Lett. **14**, 1412–1413.

Mitchell, R. H. and Liferovich, R. P. (**2004**). "A structural study of the perovskite series $Ca_{1-x}Na_xTi_{1-x}Ta_xO_3$," J. Solid State Chem. **177**, 4420–4427.

Momma, K. and Izumi, F. (**2008**). "VESTA: a three-dimensional visualization system for electronic and structural analysis," J. Appl. Crystallogr. **41**, 653–658.

Park, M., Mitchell, T. E., and Heuer, A. H. (**1975**). "Subsolidus equilibria in the TiO_2–SnO_2 system," J. Am. Ceram. Soc. **58**, 43–47.

Shannon, R. D. (**1976**). "Revised effective ionic radii and systematic studies of interatomic distances in halides and chalcogenides,"Acta Crystallogr. A **32**, 751–767.

Vegas, A., Vallet-Regí, M., González-Calbet, J. M., and Alario-Franco, M. A. (**1986**). "The $ASnO_3$ (A = Ca, Sr) perovskites" Acta Crystallogr. B **42**, 167–172.

Yamane, H. and Kawano, T. (**2011**). "Preparation, crystal structure and photoluminescence of garnet-type calcium tin titanium aluminates," J. Solid State Chem. **184**, 965–970.

Zhao, J., Ross, N. L., and Angel, R. J. (**2004**). "Tilting and distortion of $CaSnO_3$ perovskite to 7 GPa determined from single-crystal X-ray diffraction," Phys. Chem. Miner. **31**, 299–305.

Zhao, Y., Weidner, D. J., Parise, J. B., and Cox, D. E. (**1993**). "Thermal expansion and structural distortion of perovskite – data for $NaMgF_3$ perovskite. Part I," Phys. Earth Planet. Inter. **76**, 1–16.

https://doi.org/10.1017/S0885715614000074 Published online by Cambridge University Press